AD-A131 263 EVIDENCE OF EAST-WEST STRUCTURE IN LARGE-SCALE F-REGION 1/1
PLASMA ENHANCEMEN..(U) SRI INTERNATIONAL MENLO PARK CA
R T TSUNODA ET AL. 01 MAY 82 DNA-TR-82-10
UNCLASSIFIED DNA001-82-C-0021 F/G 20/9 NL

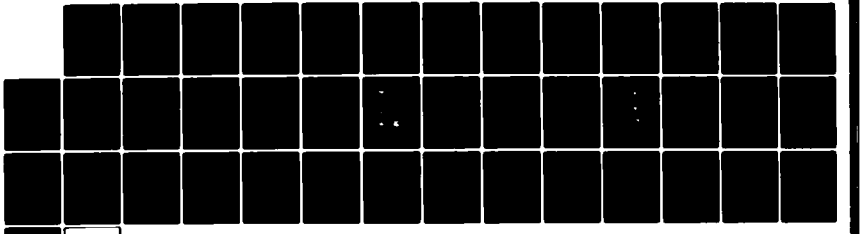

END
DATE FILMED
9 83
DTIC

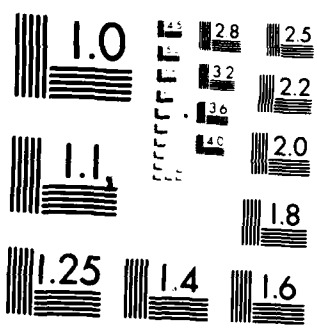

(12)

DNA-TR-82-10

AD A131263

EVIDENCE OF EAST-WEST STRUCTURE IN LARGE-SCALE F-REGION PLASMA ENHANCEMENTS IN THE AURORAL ZONE

Roland T. Tsunoda
James F. Vickrey
SRI International
333 Ravenswood Avenue
Menlo Park, California 94025

1 May 1982

Technical Report

CONTRACT No. DNA 001-82-C-0021

APPROVED FOR PUBLIC RELEASE;
DISTRIBUTION UNLIMITED.

THIS WORK WAS SPONSORED BY THE DEFENSE NUCLEAR AGENCY
UNDER RDT&E RMSS CODE B322082466 I25AAXYX00015 H2590D.

DTIC FILE COPY

Prepared for
Director
DEFENSE NUCLEAR AGENCY
Washington, DC 20305

UNCLASSIFIED

SECURITY CLASSIFICATION OF THIS PAGE (When Data Entered)

REPORT DOCUMENTATION PAGE	READ INSTRUCTIONS BEFORE COMPLETING FORM
1. REPORT NUMBER: DNA-TR-82-10	2. GOVT ACCESSION NO.: AD-A131263
3. RECIPIENT'S CATALOG NUMBER	
4. TITLE (and Subtitle): EVIDENCE OF EAST-WEST STRUCTURE IN LARGE-SCALE F-REGION PLASMA ENHANCEMENTS IN THE AURORAL ZONE	5. TYPE OF REPORT & PERIOD COVERED: Technical Report
	6. PERFORMING ORG. REPORT NUMBER: SRI Project 3984
7. AUTHOR(s): Roland T. Tsunoda James F. Vickrey	8. CONTRACT OR GRANT NUMBER(s): DNA 001-82-C-0021
9. PERFORMING ORGANIZATION NAME AND ADDRESS: SRI International, 333 Ravenswood Avenue, Menlo Park, California 94025	10. PROGRAM ELEMENT, PROJECT, TASK AREA & WORK UNIT NUMBERS: Task I25AAXYX-00015
11. CONTROLLING OFFICE NAME AND ADDRESS: Director, Defense Nuclear Agency, Washington, D.C. 20305	12. REPORT DATE: 1 May 1982
	13. NUMBER OF PAGES: 42
14. MONITORING AGENCY NAME & ADDRESS (if different from Controlling Office)	15. SECURITY CLASS (of this report): UNCLASSIFIED
	15a. DECLASSIFICATION DOWNGRADING SCHEDULE: N/A

16. DISTRIBUTION STATEMENT (of this Report)

Approved for public release; distribution unlimited.

17. DISTRIBUTION STATEMENT (of the abstract entered in Block 20, if different from Report)

18. SUPPLEMENTARY NOTES

This work was sponsored by the Defense Nuclear Agency under RDT&E RMSS Code B322082466 I25AAXYX00015 H2590D.

19. KEY WORDS (Continue on reverse side if necessary and identify by block number)

Plasma Instability
F-Region Irregularities
Gradient-Drift Instability
Auroral Irregularities

20. ABSTRACT (Continue on reverse side if necessary and identify by block number)

Large-scale (10- to 100-km) plasma-density enhancements appear to be an integral feature of the auroral F-layer ionosphere. These enhancements, called F-region "blobs," have been detected with the Chatanika incoherent-scatter radar, and are particularly noticeable during recent years of high solar activity. Blobs have attracted considerable interest because of their propensity for structuring, apparently via the gradient-drift and current-convective instabilities. Although both mechanisms predict the generation

DD FORM 1 JAN 73 1473 EDITION OF 1 NOV 65 IS OBSOLETE

UNCLASSIFIED

SECURITY CLASSIFICATION OF THIS PAGE (When Data Entered)

20. ABSTRACT (Continued)

of longitudinal structure, no measurements have been made to verify this hypothesis. In this report, we present the first direct evidence that blobs have east-west structure. The observed longitudinal structure is shown to be consistent with the production of a blob by locally intense particle precipitation at the largest scales ($\gtrsim$ 500 km) and the structuring of the blob by the gradient-drift instability at intermediate scales ($\sim$ 150 km).

EXECUTIVE SUMMARY

Evidence is presented indicating that the zonal extent of auroral F-region ionization enhancements can be comparable to their latitudinal extent. The preferred meridional wavelength of these large-scale F-region blobs is typically 50 km [e.g., Kelley et al., 1982], whereas the present observations show zonal wavelengths as short as ~150 km. Despite the fact that these east-west gradients are less steep than the meridional ones, they may still be a significant source of small-scale structure because the destabilizing meridional electric field component is typically four to five times larger than the zonal component in the auroral zone, except near the Harang discontinuity. Moreover, the linearly unstable gradient-drift mode in this configuration would result in east-west aligned sheet-like irregularities as have been observed through spaced-receiver scintillation measurements in the auroral zone [Rino et al., 1978; Livingston et al., 1978].

It is important to realize, however, that other observations (during magnetically quiet periods) have shown that some blobs extend east-west for many hundreds of kilometers. Indeed, because the F-layer production rates are relatively slow, it would seem necessary to maintain a spatial resonance between the auroral oval "source region" and the convection pattern for time periods on the order of several hours to produce the peak densities

observed. A detailed study of these effects is currently underway and will be presented elsewhere.

Because of the long lifetime of F-region ionization and rapid auroral convection speeds, the structure we observed could have been produced elsewhere. However, the two-dimensional horizontal structure observed was consistent with that expected from linear instability theory and the observed configuration of electric fields and neutral wind. This suggests that the gradient-drift instability is operative locally.

There is some inconsistency between the assumptions currently adopted in instability models/simulations and the actual auroral-zone situation. For example, the complicated effects associated with the highly conducting E layer have not been adequately addressed. We have shown the feasibility of the local operation of the gradient-drift instability in interpreting the present data set. However, if the growth rates are reduced by a factor of 10 to 100 because of the ratio of F- to E-region Pedersen conductivities, a local instability process is not viable. In that case, we suggest that structure develops principally in the polar cap, where the E-region plasma density is low, and then convects to the observation point in the auroral zone.

PREFACE

This work was supported by the Defense Nuclear Agency under Contract DNA 001-82-C-0021, and by the Air Force Office of Scientific Research under Contract F49620-80-C-0014. Radar operations were supported by the National Science Foundation under Grant ATM 7823658.

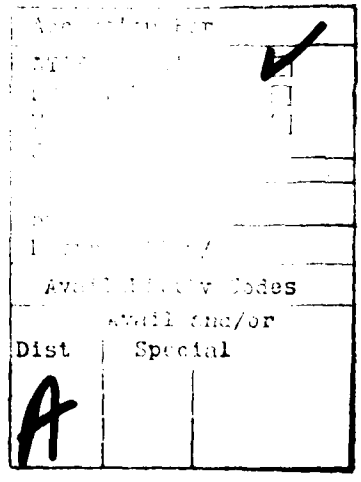

TABLE OF CONTENTS

LIST OF ILLUSTRATIONS

I INTRODUCTION

The presence of large-scale, plasma-density enhancements in the auroral F layer has become increasingly evident in recent years; their existence has been detected with the Chatanika incoherent-scatter radar [Vickrey et al., 1980; Robinson et al., 1982]. Because of the appearance of these plasma-density enhancements in isodensity-contour maps, constructed from elevation-scan data obtained in the magnetic meridian, these features have become known as F-region "blobs." These blobs, which were not very noticeable in Chatanika radar measurements during periods of low solar activity [e.g., Robinson et al., 1982], have become a dominant feature in the auroral ionosphere during recent years of high solar activity. Peak plasma densities in these enhancements range from about 10^5 el/cm^3 during solar minimum to 10^6 el/cm^3 or more during solar maximum. Blobs have spatial dimensions of about a few hundred kilometers in altitude, and from several tens of kilometers to a few hundred kilometers in latitude. They have been observed as single, isolated features or as multiple structures in the auroral zone.

Initial interpretation of radar data regarding the three-dimensional shape of blobs has been in terms of a magnetic-field-aligned slab of enhanced plasma density that extends over many degrees of longitude along an L shell, much akin to visual auroral arcs. This interpretation is natural

if blobs and visual aurora are thought of as structures produced by particle precipitation.

The existence of east-west (or longitudinal) variations in blob plasma density was not given serious consideration until the discovery that latitudinally confined regions of scintillation-producing irregularities [Fremouw et al., 1977; Rino et al., 1978; Rino and Owen, 1980] were spatially collocated with F-region blobs [Vickrey et al., 1980]. The occurrence of smaller-scale ($\lesssim$1-km) irregularities in the vicinity of horizontal gradients in plasma density associated with the walls of blobs, and the presence of an auroral electric field suggested that gradient-drift instability was probably operative as a structuring mechanism [Simon, 1963; Linson and Workman, 1970]. The occasional occurrence of small-scale irregularities on a blob wall that apparently should be stable to the gradient-drift instability has led researchers to propose current-convective instability as an alternate structuring mechanism [Ossakow and Chaturvedi, 1979; Keskinen et al., 1980].

Both the gradient-drift and current-convective instabilities predict the development of east-west structure along the walls of blobs that are characterized by latitudinally directed gradients in plasma density. Locally intense particle precipitation and sources of irregular electric fields other than the above-mentioned plasma instabilities can also produce east-west plasma-density structure. Whether one or several of these mechanisms are operative, there is good reason to expect east-west structure in F-region blobs.

In this report, we present the first direct evidence that F-region blobs do indeed have east-west plasma-density structure. A two-week experiment was conducted with the Chatanika radar in November 1981 using antenna scan modes designed so that the radar measurements would characterize the blobs in three dimensions. In addition, the electric field and meridional neutral wind were measured to determine the expected structuring configuration that would be produced by the gradient-drift instability. We selected an exceptional data set for the initial analysis and preliminary results presented here. We show that the observed structure in the blob is consistent with the gradient-drift instability driven by a southward neutral wind blowing through the equatorward wall of the blob and by a southward electric field acting on the western wall of the blob. The blob region, interpreted as being produced by soft-particle precipitation, is, therefore, envisioned as having a large quasi-elliptical cross section in the latitude-longitude plane before being distorted by the instability.

II EXPERIMENT

The Chatanika incoherent-scatter radar was operated periodically from 5 to 16 November 1981 specifically to determine the presence (or absence) of east-west horizontal structure in the auroral F layer. If such structure were discovered, we hope to characterize it in three dimensions. Because three-dimensional spatial mapping of plasma structure in a dynamic environment is extremely difficult to do with an incoherent-scatter radar, we sought to minimize space-time ambiguities by compromising on the spatial coverage sampled by the radar. Advantage was taken of the interactive capability and real-time graphic information available at the Chatanika radar facility. Various radar scan modes were designed, each intended for spatial characterization of east-west plasma structure under different electrodynamic conditions. The data set analyzed in this report was obtained using what we call the "zipzap" mode.

The zipzap mode consists of a sequence of five elevation scans in the magnetic meridian, followed by two fixed-position measurements to determine the electric-field vector and the meridional neutral wind. This mode is most suited for mapping east-west blob structure in the presence of a large zonal plasma flow. The basic approach is to scan in the meridional plane as rapidly as possible while the blob drifts eastward (or westward) through the scan plane at a measured rate. The scanned sector was restricted in

latitudinal extent to minimize the time between scans. Each scan was made in 100 s and a complete zipzap cycle was completed in 13 min.

The interactive capability of the radar was used extensively during the experiment. Elevation scans covering approximately 10^{o} of latitude at F-region altitudes were used on a patrol basis to search for blobs. Range-time-intensity (RTI) maps of the elevation scans were made in real time and used to determine blob location. The zipzap mode was then initiated with the limited-scan sector centered on the latitude of the blob(s). With this approach, we were able to track the latitudinal movement of blobs while collecting scan sequences of the blob cross section in latitude versus altitude.

The radar was operated using two pulse widths, 60 and 320 μs, which were transmitted alternately with a pulse repetition frequency of 36 s^{-1} for each pulse width. The elevation scans were continuous and covered a spatial sector corresponding to 300-km horizontal distance at an altitude of 350 km. The data were recorded on magnetic tape after a 5-s, on-line integration period. The fixed-position measurements were made for 60 s each, one with the radar beam directed to the east of the magnetic meridian for the meridional electric-field component and the other looking along the geomagnetic field line, $\vec{B}$. The second measurement gives the plasma velocity along $\vec{B}$ from which the meridional component of neutral wind can be deduced.

The plasma densities presented in this report were computed using the 320-μs pulse width and a 10-s integration period. The 10-s integration results in a 30-km horizontal distance resolution at the 350-km altitude in the meridional plane. The plasma densities were sorted into a matrix with the data columns aligned along the geomagnetic field, and then smoothed along $\vec{B}$. These smoothed data were then used to construct the isodensity contour maps presented in the following section.

III RESULTS

The data set presented in this section was obtained on 10 November 1981 between 1104 and 1117 Universal Time (UT). Alaskan Standard Time (AST) lags UT by 10 hours. The results, therefore, pertain to a period shortly after local midnight. The data set consists of six limited-sector meridian scans and corresponding electric-field and neutral-wind measurements. We present the electric-field and neutral-wind results first to establish the dynamic conditions that prevailed when the plasma-density structure was observed. We then proceed to describe the meridian-scan data and present isodensity contour maps that reveal the east-west plasma-density structure associated with F-region blobs.

The electric-field ($\vec{E}$) results are presented in Figure 1. The figure shows the (geomagnetic) southward and eastward components of the electric-field vector, plotted as a function of time. The electric-field vector was computed by combining the radial Doppler velocity measured during the elevation scans with the fixed-position measurements. Two estimates of the radial Doppler velocity out of the magnetic meridian plane were available, one obtained before the limited-sector elevation scans and the other during the period between the fifth and sixth elevation scans. The first measurement was made around 1103 UT with the antenna pointed toward geomagnetic east. The second was made around 1116 UT with the antenna

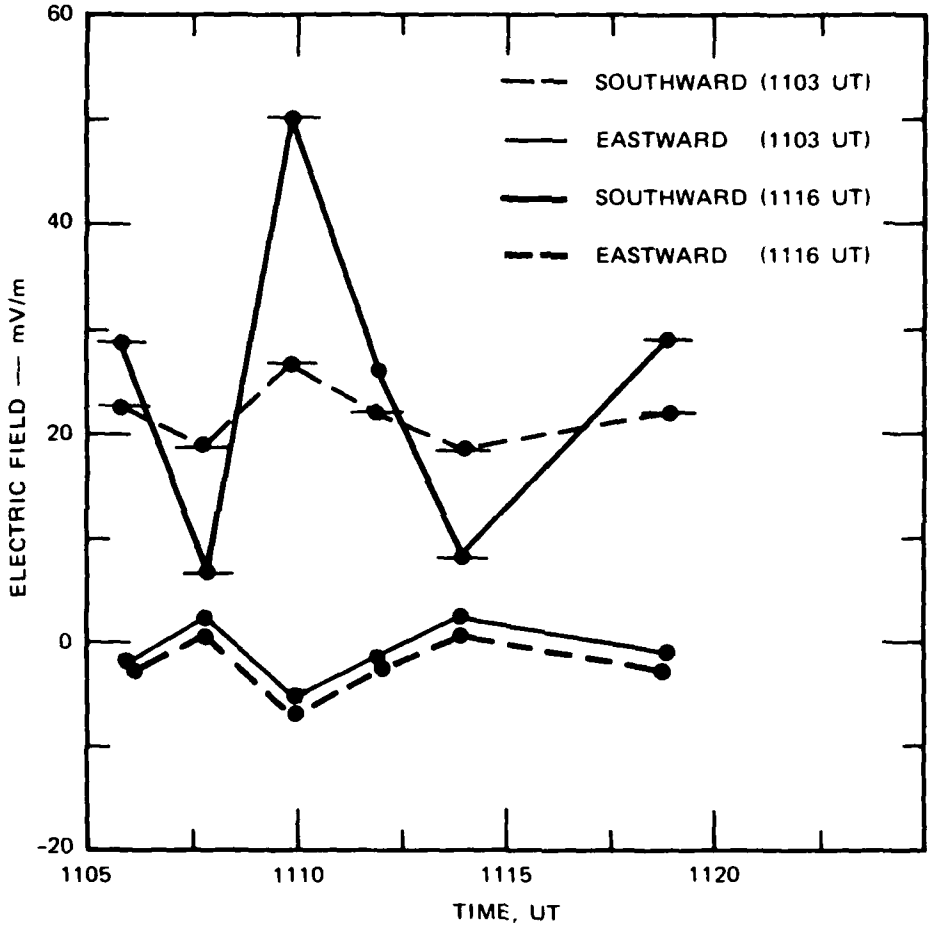

FIGURE 1 THE IONOSPHERIC ELECTRIC-FIELD VARIATIONS AS A FUNCTION OF TIME

pointed 15° east of Magnetic North and at 66° elevation. Thus, in addition to the temporal difference between the two estimates of $\vec{E}$, they are latitudinally separated. The first is more representative of the zonal drift overhead, while the second estimate of zonal drift was centered on the latitude of the blob. The results of both computations are presented in Figure 1.

The electric-field vector is important in determining the spatial location of F-region blobs as a function of time. From Figure 1, we see that the eastward electric field was small, typically 2 mV/m, and reached a maximum of -7 mV/m around 1110 UT. A 2-mV/m eastward (or westward) electric field displaces the blob only 4-km latitudinally in 100 s (the scan time); the maximum value of 7 mV/m would displace the blob 14 km in 100 s. Thus, we conclude that a blob centered in the scanned sector could not have been convected latitudinally out of that sector (±150 km) by the time of the following scan.

The southward electric field was nominally 22 mV/m, although somewhat variable with time. The zonal plasma drift during this period was, therefore, eastward at a speed of ~440 m/s (26.4 km/min). During the 100 s it took to complete an elevation scan, a blob could have moved 44 km in longitude. With this sampling rate, therefore, we cannot resolve east-west structure with scale sizes less than 88 km.

Knowledge of the electric field is also important (together with the neutral wind) for estimating the growth rate of the gradient-drift

instability. East-west structure can be produced by that instability when a north-south component of the difference (or "slip") velocity between the F-region plasma and the neutral gas exists. The meridional component of the neutral wind was ~380 m/s at 1103 UT and ~370 m/s at 1117 UT, both directed southward. The slip velocity, therefore, must have been in the range from 230 m/s to 420 m/s, and directed poleward. With this slip-velocity direction, the equatorward wall of a blob should have been unstable and, thus, subject to east-west plasma structuring.

We now describe the meridian-scan data set, presented in Figure 2. The first five panels [Figures 2(a) to 2(e)] contain isodensity contour maps of the auroral ionosphere above the 200-km altitude, obtained between the times of the neutral-wind measurements. The fifth scan [Figure 2(e)] was followed by electric-field and neutral-wind measurements, and then the sixth scan shown in Figure 2(f). The isodensity contours are plotted in a format such that the geomagnetic field is vertical in the altitude versus invariant-latitude coordinates. The magnetic dip angle at Chatanika is 76.9^{o} at the 300-km altitude. Heavy lines have been used for contours with values of 4, 6, 8, and 10 x 10^5 el/cm^3. The first five scans were made at approximately 2-min intervals, and the sixth scan was completed about 5 min after the fifth scan.

The blobs can be characterized by their peak plasma density, altitude of peak plasma density, and latitudinal gradient. The peak plasma density is seen to vary from 4 x 10^5 el/cm^3 to 1.1 x 10^6 el/cm^3. The largest of these values is about two times greater than that reported by

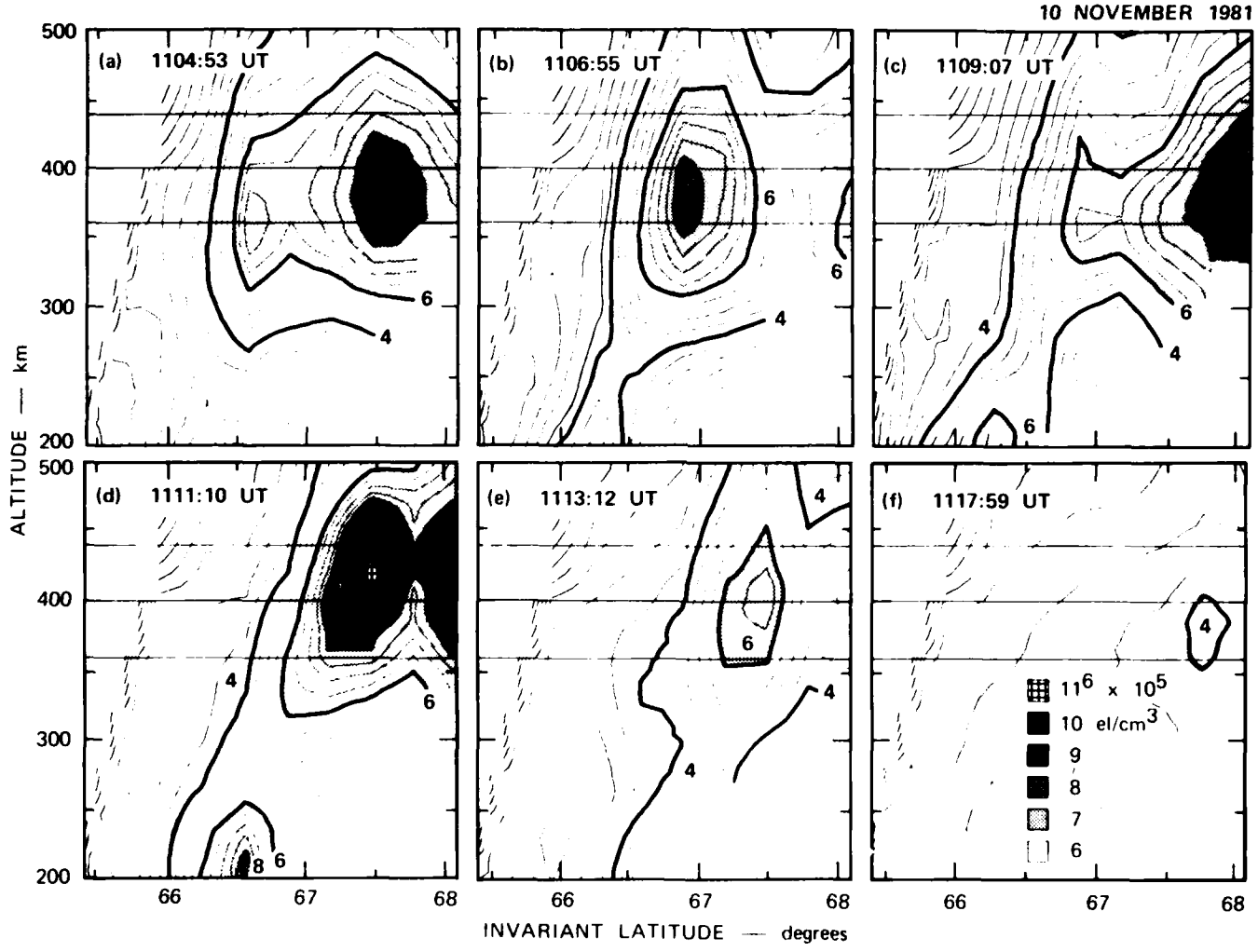

FIGURE 2 SIX MERIDIAN-SCAN MAPS OF ISODENSITY CONTOURS SHOWING THE VARIABILITY IN BLOB PLASMA-DENSITY STRUCTURE

Vickrey et al. [1980]. The altitude of maximum plasma density is somewhat variable, ranging from 380 to 420 km. These plasma densities and F-layer peak altitudes are in reasonable agreement with the computational results of Watkins and Richards [1979]. Using a soft-particle precipitation model, they found that an equatorward-directed neutral wind increases both the altitude of the F-layer peak and the peak plasma density. Finally, we note that the latitudinal plasma-density gradient is steeper on the equatorward side of the blob. A steeper equatorward wall is consistent with our prediction of gradient-drift structuring based on the electrodynamic conditions described above.

Beside the physical characteristics of blobs seen in a given contour map, important evidence for east-west structure is contained in the variability of blob characteristics from map to map. From Figure 2, we see that blobs found in successive maps do not correlate well. A blob found in one map cannot be easily identified with a blob in the next map without involving an anomalously large (1) production by particle precipitation, (2) latitudinal transport by east-west electric fields, or (3) loss rate. The only reasonable interpretation appears to be in terms of east-west structure.

For example, the blob in Figure 2(a) at the 380-km altitude might be associated with the intense blob in Figure 2(b) if both anomalously large production and equatorward transport occurred between scans. Watkins and Richards [1979] showed, however, that the e-folding time for F-region plasma-density production by particle precipitation is about one hour. Even

if anomalously large production rates were not needed, we find that the observed latitudinal displacement requires a westward electric field of about 30 mV/m. The westward electric field was not larger than 3 mV/m.

Other examples can be found in Figure 2. The intense blob in Figure 2(b) could have decayed or moved latitudinally out of the scanned sector by the time of the scan corresponding to Figure 2(c). At a nominal altitude of 400 km, the e-folding decay time is about 16 hours. With this extremely slow decay rate, the peak plasma density of 8×10^5 el/cm^3 [Figure 2(b)] should not have decayed by more than 0.25 percent in the time between scans. We see from Figure 2(c), however, that the peak plasma density was $\sim 6.5 \times 10^5$ el/cm^3, which corresponds to a 20 percent decrease. Moreover, we note that the poleward displacement would require an eastward electric field of 50 mV/m. The measured eastward electric field was smaller by more than an order of magnitude.

As a final example, the changes in the blob seen in each of the maps in the bottom row of Figure 2 could reasonably be interpreted in terms of latitudinal transport. The decay rate, however, is unreasonable. The peak plasma density of the blob in Figure 2(f) should not have decayed to less than 9×10^5 el/cm^3. Instead, we find that the peak plasma density has decreased to about 4×10^5 el/cm^3. This apparent rapid decay, however, could have easily been produced by an east-west gradient scale length of 120 km moving zonally at 440 m/s.

Interpretation of the data in Figure 2 in terms of east-west structure is best illustrated by plan views of the isodensity contours at selected altitudes. To do this, we have taken the plasma-density variations as a function of invariant latitude, at selected altitudes (horizontal lines in the maps in Figure 2), and fitted isodensity contours to the values obtained from the six scans. The zonal displacements between scans were computed by using the measured southward electric field of 22 mV/m. No attempt was made to compensate for any latitudinal displacement because the east-west electric field was small. The resulting isodensity contour maps for altitudes of 360, 400, and 440 km are presented in Figure 3.

Analysis of the contour maps in Figure 3 reveals three important features. First, the lower-valued isodensity contours (e.g., 5×10^5 el/cm^3) are aligned northwest-southeast, instead of along a contour of constant invariant latitude. Such a tilt could have been produced by a 6-mV/m eastward electric field. However, the fact that the zonal electric-field component was westward on average suggests that the tilted contours simply outline a large region of enhanced plasma density produced by localized particle precipitation. The abrupt termination of the blob at the west end of the maps provides more conclusive evidence that the tilt is actual spatial structure.

To determine the total east-west extent of the enhanced plasma-density region produced (presumably) by locally intense particle precipitation, we examined elevation-scan data taken before to the first scan in Figure 2. In a full-elevation scan made from 1052:44 to 1101:00 UT, a blob was detected

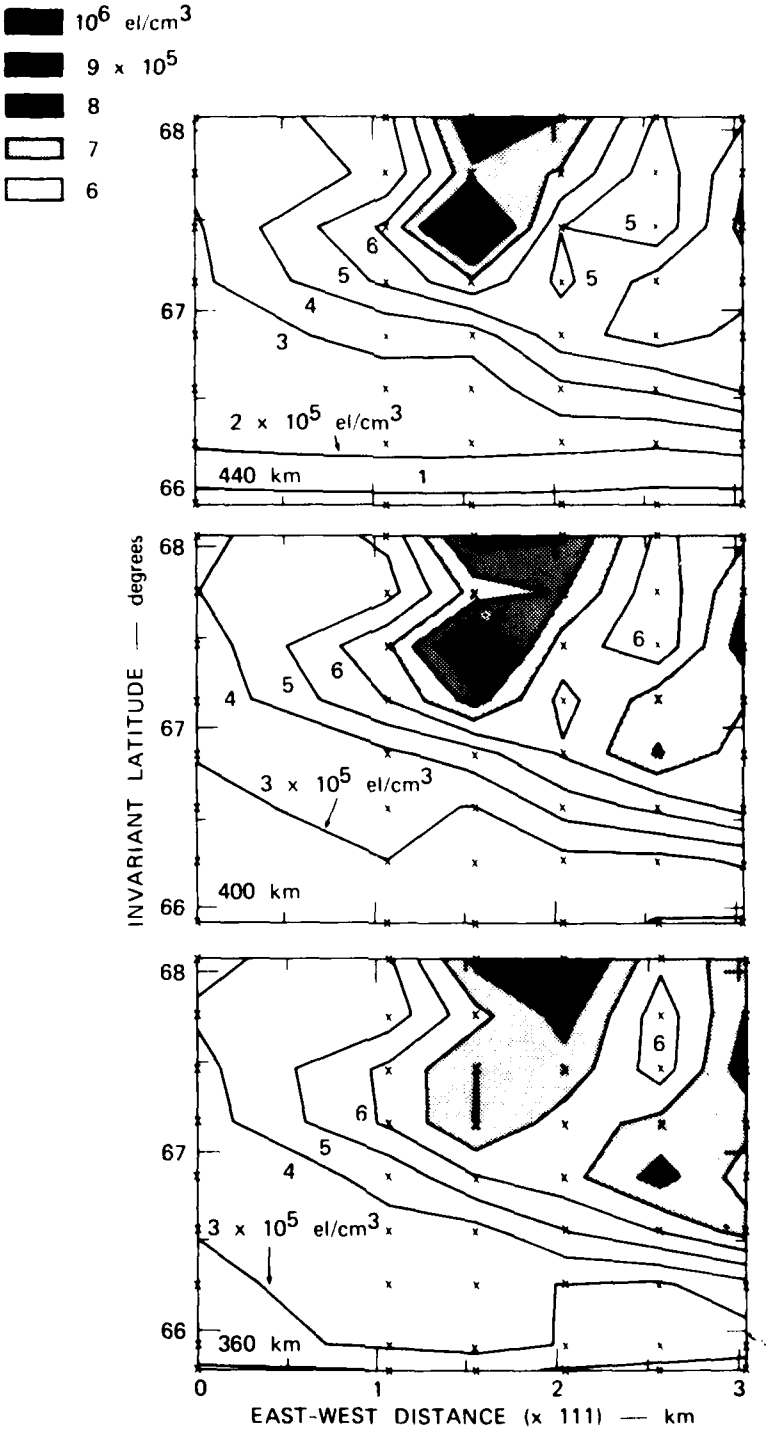

FIGURE 3 PLAN VIEWS OF BLOB EAST-WEST STRUCTURE AT THREE DIFFERENT ALTITUDES

at 67.6° invariant latitude and at the 350-km altitude. The peak plasma density of the blob was 1.3 x 10^6 el/cm^3. In an even earlier scan, made from 1040:32 to 1048:48 UT, a blob was not seen near this latitude. Using an average southward electric field of 15 mV/m (the southward electric field was 10 mV/m at 1041 UT), we estimate that the eastern boundary of the blob must have extended about 400 km to the right of the contour maps in Figure 3. The full east-west extent of the blob, therefore, must have been close to 600 km.

From the above analysis, we envision all of the F-region blobs in Figure 2 as parts of a single, large-scale region of enhanced plasma density, perhaps similar in cross section to an ellipse with the major axis oriented in the geomagnetic east-west direction and having a 600-km extent. The portion of the ellipse seen in Figure 3 would be the southwest quadrant of the elliptically shaped blob. In this interpretation, the tilted, lower-isodensity contours in Figure 3 can be thought of as describing the ellipse. The north-south extent is not completely sampled, but is at least 300 km. This large region of enhanced plasma density, presumably produced by locally intense particle precipitation, is imbedded in a background F-layer plasma density of perhaps 2 x 10^5 el/cm^3.

The second feature of interest in the contour maps of Figure 3 is the pattern created by the higher-valued isodensity contours. Two regions of enhanced plasma density are seen to have a form like "fingers" extending southward and to be separated in east-west direction by regions of depleted plasma density. Similar patterns of east-west structure are seen in the

three contour maps taken at different altitudes. The east-west separation of the fingers is about 150 km. The enhanced (and depleted) plasma density regions are also characterized by a tilt away from Magnetic North (vertical direction in Figure 3) i.e., the major axis of the enhancements are aligned northeast-southwest. The alignment of the enhancements (and depletions) are nearly orthogonal to the lower-valued isodensity contours (first feature).

The plasma density in the center finger (at the 400- and 440-km altitudes) exceeds 10^6 el/cm^3 by about a factor of two greater than that in the depleted region along its east side. The peak plasma density in the east finger, however, is smaller than that in the center finger. This difference cannot be explained by flux-tube interchange processes such as those associated with the gradient-drift instability without assuming some initial structure produced by locally intense particle precipitation.

Finally, the third feature of interest is an apparent structuring of the west wall of the center finger in Figure 3. The structure is in the form of an eastward penetration of a low plasma-density contour between two regions of higher plasma density. This structure is most evident at the 400-km altitude, although there is also some evidence of the eastward penetration (of a lower-valued contour) at the 360 km altitude. West-wall structuring is consistent with the gradient-drift instability driven by a southward electric field.

To summarize, the blobs observed during the six scans in Figure 2 are clearly not latitudinal cross sections of independent plasma-density structures that are uniformly extended in longitude. The variations of the blobs in latitudinal location and peak plasma density cannot be explained in terms of latitudinal transport by the measured electric fields nor by reasonable production or decay rates of plasma density. The simplest and most consistent interpretation of the data in Figures 2 and 3 is that a single large-scale blob was originally produced with a quasi-elliptical cross section (600 km in longitude, $\gtrsim$300 km in latitude), by locally intense particle precipitation. That initial configuration was then structured zonally along its equatorward wall by the gradient-drift instability on an intermediate scale (~150 km). The observed north-south structure is also consistent with that produced by the same instability.

Of course, the F-region plasma configuration does not have to be locally unstable to produce the structure we have observed. Indeed, the original precipitation structure itself may be quite complicated. Moreover, the long lifetime of F-region ionization and relatively slow cross-field diffusive decay rates lead to the situation where structural evolution is cumulative. In other words, the amount of structure observed on a given set of flux tubes depends in a complicated way on the structuring influences encountered by those flux tubes during their past history [e.g., Vickrey and Kelley, 1982a]. Nevertheless, the fact that the observed structure consistently agrees with that expected from the local dynamics is highly suggestive that local instabilities are indeed operating.

IV DISCUSSION AND CONCLUSIONS

We have presented a data set in which the spatial distribution of the observed F-region plasma density can most easily be explained in terms of a single, large-scale plasma blob having significant east-west structure. The blob itself was interpreted as being initially produced by locally intense particle precipitation at the largest horizontal scales (~300 by 600 km), and being structured by the gradient-drift instability at smaller scales (~150 km). Although the smaller-scale structure could, in principle, also be interpreted as being produced by locally intense particle precipition, the characteristics of this structure are consistent with that of structure produced by the gradient-drift instability. That is, in the presence of a poleward-directed slip velocity between F-region ions and neutrals, (1) steeper latitudinal gradients in plasma density were found along the equatorward side of blobs, and (2) the intermediate-scale structure appeared to be associated with the equatorward side of the enhanced plasma-density region. We note that the current-convective instability [Ossakow and Chaturvedi, 1979] does not have to be invoked to explain these observations because the slip velocity, controlled by a southward-directed neutral wind, was directed poleward. The current-convective instability contributes a destabilizing factor to the irregularity growth rate; however, that factor acts on both the poleward and equatorward gradients and, hence, does not alter the basic conclusions.

In the case of an isolated F-region blob, whose density dominates the height-integrated Pedersen conductivity of the flux tube, the linear growth rate of the gradient-drift instability can be estimated for simple slab geometry from the results of Linson and Workman [1970]. (This conventional formula, applied originally to barium ion-cloud structuring at lower altitudes, has been shown by Ossakow et al. [1977] to be valid at the altitudes and conditions of this data set.) In our case, for a southward neutral wind of 370 m/s acting on a mean plasma-density gradient with scale length of ~50 km, the irregularity e-folding growth time is 2.3 min. This growth rate would appear large enough to have produced the pattern of east-west structure presented in Figure 3. For example, if the initial perturbation amplitude was 1 km, the observed wave amplitude of about 150 km would have occurred in a period of seven e-folding times, or about 15 min.

While the southward neutral wind acted on the northward-directed gradient to produce the east-west structure, the southward electric field should have acted on the eastward-directed gradient to produce north-south structure. A 22-mV/m electric field acting on a 120-km gradient scale length gives an e-folding time of 4.5 min. However, the zonal neutral wind is not known. Its contribution to the slip velocity will determine the actual e-folding time. The observed eastward penetration of lower-valued isodensity contours into the center enhancement in Figure 3 is consistent with our expectation that the zonal neutral wind was less eastward than the bulk plasma motion. The neutral wind, determined primarily by ion drag, would have been directed westward in the premidnight sector until the reversal in plasma flow (in the Harang discontinuity region). Its

subsequent eastward velocity would be expected to lag that of the plasma. The relative lack of structure along the west wall of the east finger (right side of Figure 3) as compared to the center finger, also supports the concept that north-south structuring of the center finger occurred simultaneously with east-west structuring, i.e., no secondary process is required.

The above discussion of gradient-drift structuring in the two orthogonal directions as independent processes may not be realistic. Perkins and Doles [1975] and Keskinen and Ossakow [1982] showed that for a slab geometry, the electric-field component parallel to the gradient can act to dampen the irregularity growth rate of the gradient-drift instability. The stabilization results from a shear in the $\vec{E} \times \vec{B}$ velocity, because the electric field along the plasma-density (conductivity) gradient must necessarily be locally intense to maintain a horizontally divergence-free current. The velocity shear produced in their treatment also acts to tilt the structures in the sense dictated by slower velocities in higher plasma-density regions. For our data set where the southward electric field is antiparallel to the plasma-density gradient, the east-west structures would be expected to be rotated counterclockwise in Figure 3 from the direction perpendicular to the initial gradient if the velocity-shear mechanism is valid.

The alignment of the east-west structure in Figure 3 is seen to be roughly orthogonal to the direction of the plasma-density gradient. The absence of a tilt in the fingers suggests that the velocity-shear mechanism

is not operative. Its absence in the auroral ionosphere, however, is expected. The requirement for a divergence-free current in the F layer can be satisfied by field-aligned currents that close in a highly conducting auroral E layer. Further discussion of the effects of conducting background on the gradient-drift instability is given in later paragraphs.

The observed spatial wavelength of 150 km in east-west structure also deserves some discussion. Keskinen et al. [1980] suggested that the outer scale of gradient-drift-produced structure is always comparable to the initial gradient scale length. This prediction, made on the basis of numerical simulations of an isolated (i.e., no E region) plasma-cloud model, would appear to be borne out by our observations. The spatial wavelength of 150 km is only three times the estimated gradient scale length.

All of the theoretical work mentioned above is strictly valid only for an F-region blob that is insulated from a conducting E layer or background ionosphere. More precisely, it is assumed that the integrated Pedersen conductivity along magnetic flux tubes through the F-region blob is much greater than the flux-tube-integrated Pedersen conductivity of the background ionosphere. Although the E-region measurements corresponding to this data set were not available, this assumption is not usually valid in the auroral zone. For example, Vickrey et al. [1980] showed that the ratio of integrated Pedersen conductivity between the E and F layers can be as large as a factor of 100. Moreover, we have seen from Figure 3 that the background F-layer plasma density is only two to three times smaller than the peak plasma density within the blob. The presence of a conducting

background, particularly that of an auroral E layer, leads to several complications.

Perhaps the most obvious effect of a conducting E layer is that of polarization charge neutralization by field-aligned currents that close in the E layer. Because polarization electric fields are responsible for driving the gradient-drift instability as well as the velocity shear mechanism [Perkins and Doles, 1975], we expect a strong reduction of the gradient-drift growth rate and suppression of the velocity shear in the presence of an auroral E layer. As a first guess, we would expect the growth rate to be proportional to $(1 + \lambda)$ where λ = ratio of the integrated Pedersen conductivity of the blob to that of the background ionosphere (primarily the E layer). Shiau and Simon [1974] analyzed shorting effects of a conducting background and found that all modes for the barium ion cloud case are stable for λ slightly less than 0.5. The critical value of λ for the auroral F-region blob case should be lower because blobs occur at higher altitudes and because larger electric fields and neutral winds are found in the auroral zone, compared to values used by Shiau and Simon [1974]. The growth time required to produce the observed east-west structure, therefore, is likely to have been much longer than a few tens of minutes. The virtual absence of tilts in the east-west structure also is consistent with the expected effects of a conducting E layer mentioned above.

Many other complications of auroral F-layer instabilities remain to be sorted out. A highly conducting E layer can lead to cross-field diffusion of the F region at the ion rate rather than at the electron (or

ambipolar-diffusion) rate because electrons can move freely up and down field lines to and from the E layer where the ion gas is compressible [Simon, 1955, Vickrey and Kelley, 1982b]. On the other hand, the compressibility of the E-region plasma allows images of F-region structure to form in the E layer (at least at small scales), which retards diffusion at those scales in the F layer. Image effects have been considered by Volk and Haerendel [1971]; Goldman et al. [1974]; Scannapieco et al. [1974]; Francis and Perkins [1975]; Doles et al. [1976]; and Vickrey and Kelley [1982b]. Assessment of the ultimate impact of E-region images on F-layer instabilities will require further theoretical work. For example, the fact that E-region images must grow by compressing the ion gas faster than it is recombined by chemistry, means that the formation of images depends on scale size [see, for example, the discussion by Vickrey and Kelley, 1982b]. Smaller-scale images grow faster than large-scale images. However, the efficiency with which the image "source" electric-field maps from the F layer to the E region decreases rapidly at small scale sizes. These competing effects may lead to a preferred scale size of irregularities in both the E and F layers. Moreover, important effects are associated, with the fact that for a given driving electric field, F-layer irregularities drift rapidly in the Hall direction, whereas the E-region ion gas that is compressed to form images, drifts substantially in the Pedersen direction. Another complicating effect for E-region images is that the auroral E-region density may be already structured on scale sizes comparable to the image size because of structured particle precipitation. To date, no theoretical investigation has treated all of these mechanisms together.

In summary, direct evidence has been presented for the presence of east-west structure in F-region plasma-density enhancements, or blobs. The spatial dimensions of the blob analyzed in this data set however, should not necessarily be considered typical. Other observations have shown that blobs can extend in longitude over many hundreds of kilometers. Moreover, we do not know whether structuring always occurs with a preferred wavelength of 150 km. A more complete investigation of blob characterization is underway and will be the topic of future reports.

The interpretation of the data set presented as being consistent with ongoing structuring via the gradient-drift process must also be viewed with caution. Although the interpretation is qualitatively consistent with theory, we must recognize the possibility of complicating contributions. For example, it is conceivable that significant structuring via the gradient-drift instability is not possible in the auroral zone (because of the conducting E layer) and that the observed structure is produced by other means or elsewhere (e.g., nighttime polar cap) where E-region conductivity effects are less significant.

REFERENCES

Doles, J. H., N. J. Zabusky, and F. W. Perkins, "Deformation and Striation of Plasma Clouds in the Ionosphere, 3. Numerical Simulations of a Multilevel Model with Recombination Chemistry," J. Geophys. Res., 81, 5987, 1976.

Francis, S. H., and F. W. Perkins, "Determination of Striation Scale Sizes for Plasma Clouds in the Ionosphere," J. Geophys. Res., 82, 3111, 1975.

Fremouw, E. J., C. L. Rino, R. C. Livingston, and M. C. Cousins, "A Persistent Subauroral Scintillation Enhancement Observed in Alaska," Geophys. Res. Lett., 4, 539, 1977.

Goldman, S. R., S. L. Ossakow, and D. L. Book, "On the Nonlinear Motion of a Small Barium Cloud in the Ionosphere," J. Geophys. Res., 79, 1471, 1974.

Kelley, M. C., C. W. Carlson, and R. Torbert, "On the Origin and Spatial Extent of High-Latitude F-Region Irregularities," J. Geophys. Res., in press, 1982.

Keskinen, M. J., and S. L. Ossakow, "Nonlinear Evolution of Plasma Enhancements in the Auroral Ionosphere, 1: Long Wavelength Irregularities," J. Geophys. Res., 87, 144, 1982.

Keskinen, M. J., S. L. Ossakow, and B. E. McDonald, "Nonlinear Evolution of Diffuse Auroral F Region Ionospheric Irregularities," Geophys. Res. Lett., 7, 573, 1980.

Keskinen, M. J., B. E. McDonald, and S. L. Ossakow, "Preliminary Numerical Study of the Outer Scale Size of Ionospheric Plasma Cloud Striations," J. Geophys. Res., 85, 2349, 1980.

Linson, L. M., and J. B. Workman, "Formation of Striations in Ionosheric Plasma Clouds," J. Geophys. Res., 75, 3211, 1970.

REFERENCES (continued)

Livingston, R. C., C. L. Rino, J. Owen, and R. T. Tsunoda, "The Anisotropy of High-Latitude Nighttime F-Region Irregularities," Topical Report, Contract DNA 001-81-C-076, SRI Project 2326, SRI International, Menlo Park, CA (April 1982).

Ossakow, S. L., and P. K. Chaturvedi, "Current Convective Instability in the Diffuse Aurora," Geophys. Res. Lett., 6, 332, 1979.

Ossakow, S. L., P. K. Chaturvedi, and J. B. Workman, "High Altitude Limit of the Gradient Drift Instability," NRL Memorandum Report 3639, Naval Research Laboratory, Washington, D.C. (November 1977).

Perkins, F. W., and J. H. Doles, III, "Velocity Shear and the E x B Instability," J. Geophys. Res., 80, 211, 1975.

Rino, C. L., and J. Owen, "The Structure of Localied Nighttime Auroral-Zone Scintillation Enhancements," J. Geophys. Res., 85, 2941, 1980.

Rino, C. L., R. C. Livingston, and A. J. Matthews, "Evidence for Sheet-Like Auroral Ionosheric Irregularities," Geophys. Res. Letters, 5, 1039, 1978.

Robinson, R. M., R. R. Vondrak, and T. A. Potemra, "Electrodynamic Properties of the Evening-Sector Ionosphere Within the Region 2 Field-Aligned Current Sheet," J. Geophys. Res., 87, 731, 1982.

Scannapieco, A. J., S. L. Ossakow, D. L. Book, B. E. McDonald, and S. R. Goldman, "Conductivity Ratio Effects on the Drift and Deformation of F Region Barium Clouds Coupled to the E Region Ionosphere," J. Geophys. Res., 79, 2913, 1974.

Shiau, J., and A. Simon, "Barium Cloud Growth and Striation in a Conducting Background," J. Geophys. Res., 79, 1895, 1974.

Simon, A., "Instability of a Partially Ionized Plasma in Crossed Electric and Magnetic Fields," Phys. Fluids, 6, 382, 1963.

REFERENCES (concluded)

Simon, A., "Ambipolar Diffusion in a Magnetic Field," Phys. Rev., 98, 317, 1955.

Vickrey, J. F., and M. C. Kelly, "Irregularities and Instabilities in the Auroral F Region," in High-Latitude Space Plasma Physics, Plenum Publishing Corp., New York, NY, in press, 1982a.

Vickrey, J. F., and M. C. Kelley, "The Effects of a Conducting E-Layer on Classical F-Region Cross-Field Plasma Diffusion," J. Geophys. Res., accepted for publication, 1982b.

Vickrey, J. F., C. L. Rino, and T. A. Potemra, "Chatanika/TRIAD Observations of Unstable Ionization Enhancements in the Auroral F Region," Geophys. Res. Lett., 7, 789, 1980.

Volk, H. F., and G. Haerendel, "Striations in Ionosheric Ion Clouds, 1," J. Geophys. Res., 76, 4541, 1971.

Watkins, B. J., and P. G. Richards, "A Theoretical Investigation of the Role of Neutral Winds and Particle Participation in the Formation of the Auroral F-Region Ionosphere," J. Atmos. Terr. Phys., 41, 179, 1979.

DISTRIBUTION LIST

DEPARTMENT OF DEFENSE

Assistant to the Secretary of Defense
Atomic Energy
ATTN: Executive Asst

Command & Control Tech Ctr
ATTN: C-650, G. Jones
ATTN: C-650
ATTN: C-312, R. Mason
3 cy ATTN: C-650, W. Heidig

Defense Communications Agency
ATTN: Code 230
ATTN: Code 205
ATTN: J300 for Yen-Sun Fu

Defense Communications Engineer Center
ATTN: Code R410
ATTN: Code R410, R. Craighill
ATTN: Code R123
ATTN Code R410, N. Jones

Defense Intelligence Agency
ATTN: DB-4C, E. O'Farrell
ATTN: DC-7B
ATTN: DB, A. Wise
ATTN: DT-1B
ATTN: DIR

Defense Nuclear Agency
ATTN: STNA
ATTN: NAFD
ATTN: RAEE
ATTN: NATD
ATTN: RAAE, P. Lunn
3 cy ATTN: RAEE
4 cy ATTN: TITL

Defense Tech Info Ctr
12 cy ATTN: DD

Dep Under Secretary of Defense
Comm, Cmd, Cont & Intell
ATTN: Dir of Intell Sys

Field Command
DNA Det 1
Lawrence Livermore Lab
ATTN: FC-1

Field Command
Defense Nuclear Agency
ATTN: FCTXE
ATTN: FCTT, G. Ganong
ATTN: FCTT, W. Summa
ATTN: FCPR

Interservice Nuc Weapons School
ATTN: TTV

Joint Chiefs of Staff
ATTN: C3S
ATTN: C3S Evaluation Office, HDOO

Joint Strat Tgt Planning Staff
ATTN: JLA, Threat Applications Div
ATTN: JLTW-2

DEPARTMENT OF DEFENSE (Continued)

National Security Agency
ATTN: R-52, J. Skillman
ATTN: B-3, F. Leonard
ATTN: W-32, O. Bartlett

Under Secy of Def for Rsch & Engrg
ATTN: Strat & Space Sys, OS
ATTN: Strat & Thtr Nuc Forces, B. Stephan

WWMCCS System Engineering Org
ATTN: J. Hoff

DEPARTMENT OF THE ARMY

Assistant Ch of Staff for Automation & Comm
ATTN: DAMO-C4, P. Kenny

US Army Electronics R&D Command
ATTN: DELAS-EO, F. Niles

BMD Advanced Tech Ctr
ATTN: ATC-R, W. Dickinson
ATTN: ATC-O, W. Davies
ATTN: ATC-T, M. Capps
ATTN: ATC-R, D. Russ

BMD Systems Command
ATTN: BMDSC-HLE, R. Webb
2 cy ATTN: BMDSC-HW

Dep Ch of Staff for Ops & Plans
ATTN: DAMO-RQC, C2 Div

Harry Diamond Labs
ATTN. DELHD-NW-P
ATTN: DELHD-NW-R, R. Williams

US Army Chemical School
ATTN: ATZN-CM-CS

US Army Comm-Elec Engrg Instal Agency
ATTN: CCC-EMEO-PED, G. Lane
ATTN: CCC-CED-CCO, W. Neuendorf

US Army Communications Command
ATTN: CC-OPS-W
ATTN: CC-OPS-WR, H. Wilson

US Army Foreign Science & Tech Ctr
ATTN: DRXST-SD

USA Missile Command
ATTN: DRSMI-YSO, J. Gamble

US Army Materiel Dev & Readiness Cmd
ATTN: DRCLDC, J. Bender

US Army Nuc & Chem Agency
ATTN: Library

US Army Satellite Comm Agency
ATTN: Doc Control

DEPARTMENT OF THE ARMY (Continued)

US Army Communications R&D Command
ATTN: DRDCO-COM-RY, W. Kesselman

US Army TRADOC Sys Analysis Actvy
ATTN: ATAA-TDC
ATTN: ATAA-TCC, F. Payan Jr
ATTN: ATAA-PL

DEPARTMENT OF THE NAVY

Joint Cruise Missiles Project Ofc
ATTN: JCMG-707

Naval Air Systems Command
ATTN: PMA 271

Naval Electronic Systems Command
ATTN: Code 3101, T. Hughes
ATTN: PME-117-2013, G. Burnhart
ATTN: PME 106-13, T. Griffin
ATTN: Code 501A
ATTN: PME 106-4, S. Kearney
ATTN: PME 117-20
ATTN: PME 117-211, B. Kruger

Naval Intelligence Support Ctr
ATTN: NISC-50

Naval Ocean Systems Center
ATTN: Code 532
ATTN: Code 5323, J. Ferguson
ATTN: Code 5322, M. Paulson

Naval Research Lab
ATTN: Code 4720, J. Davis
ATTN: Code 4780, S. Ossakow
ATTN: Code 4700
ATTN: Code 4780
ATTN: Code 7500, B. Wald
ATTN: Code 6700
ATTN: Code 7950, J. Goodman
ATTN: Code 4187

Naval Space Surveillance System
ATTN: J. Burton

Naval Surface Weapons Ctr
ATTN: Code F31

Naval Telecomm Command
ATTN: Code 341

Ofc of the Deputy Chief of Naval Ops
ATTN: OP 941D
ATTN: NOP 654, Strat Eval & Anal Br
ATTN: OP 981N

Office of Naval Research
ATTN: Code 414, G. Joiner
ATTN: Code 412, W. Condell

Strat Sys Project Office
ATTN: NSP-2722, F. Wimberly
ATTN: NSP-43
ATTN: NSP-2141

Theater Nuc Warfare Prj Office
ATTN: PM-23, D. Smith

DEPARTMENT OF THE AIR FORCE

Air Force Geophysics Lab
ATTN: OPR, H. Gardiner
ATTN: OPR-1
ATTN: LKB, K. Champion
ATTN: CA, A. Stair
ATTN: PHY, J. Buchau
ATTN: R. Babcock
ATTN: R. O'Neil

Air Force Tech Applications Ctr
ATTN: TN

Air Force Weapons Lab
ATTN: SUL
ATTN: NTYC
ATTN: NTN

Air Force Wright Aeronautical Lab
ATTN: A. Johnson
ATTN: W. Hunt

Air Logistics Command
ATTN: OO-ALC/MM

Air University Library
ATTN: AUL-LSE

Assistant Ch of Staff
Studies & Analyses
ATTN: AF/SASC, C. Rightmeyer
ATTN: AF/SASC, W. Kraus

Ballistic Missile Office
ATTN: ENSN, W. Wilson
ATTN: SYC, Col Kwan

Deputy Ch of Staff
Research, Development, & Acq
ATTN: AFRDS, Space Sys & C3 Dir
ATTN: AFRDSS
ATTN: AFRDSP

Deputy Chief of Staff, Plans & Ops
ATTN: AFXOKT
ATTN: AFXOKCD
ATTN: AFXOKS

Electronic Systems Div
ATTN: ESD/SCTE, J. Clark

Electronic Systems Div
ATTN: OCT-4, J. Deas

Electronic Systems Div
ATTN: SCS-1E
ATTN: SCS-2, Lt Col, Vinkels

Foreign Tech Division
ATTN: NIIS Library
ATTN: TQTD, B. Ballard

Rome Air Development Ctr
ATTN: TSLD
ATTN: OCS, V. Coyne

Rome Air Development Ctr
ATTN: EEP, J. Rasmussen

DEPARTMENT OF THE AIR FORCE (Continued)

Space Command
ATTN: DC, T. Long

Space Division
ATTN: YGJB, W. Mercer
ATTN: YKM, Maj Alexander
ATTN: YKM, Cpt Norton

Strat Air Command
ATTN: NRT
ATTN: DCX
ATTN: XPFS
ATTN: Adwate, B. Bauer
ATTN: DCXT, T. Jorgensen

DEPARTMENT OF ENERGY

Department of Energy
ATTN: DP-233

OTHER GOVERNMENT AGENCIES

Central Intelligence Agency
ATTN: OSWP/SSD for K. Feuerpfetl
ATTN: OSWR/NED

Department of Commerce
National Bureau of Standards
ATTN: Sec Ofc for R Moore

Department of Commerce
National Oceanic & Atmospheric Admin
ATTN: R. Grubb

Institute for Telecommunications Sciences
ATTN: W. Utlaut
ATTN: A. Jean
ATTN: L. Berry

NATO

NATO School, SHAPE
ATTN: US Documents Officer

DEPARTMENT OF ENERGY CONTRACTORS

EG&G, Inc
ATTN: D. Wright
ATTN: J. Colvin

University of Calfornia
Lawrence Livermore National Lab
ATTN: Tech Info Dept Library
ATTN: L-389, R. Ott
ATTN: L-31, R. Hager

Los Alamos National Lab
ATTN: MS 664, J. Zinn
ATTN: P. Keaton
ATTN: D. Simons
ATTN: MS 670, J. Hopkins
ATTN: T. Knukle, ESS-5
ATTN: R. Jeffries
ATTN: J. Wolcott
ATTN: C. Westervelt

Sandia National Labs, Livermore
ATTN: T. Cook
ATTN: B. Murphey

DEPARTMENT OF ENERGY CONTRACTORS (Continued)

Sandia National Lab
ATTN: Space Project Div
ATTN: D. Dahlgren
ATTN: D. Thronbrough
ATTN: Tech Lib 3141
ATTN: ORG 4231, T. Wright
ATTN: ORG 1250, W. Brown

DEPARTMENT OF DEFENSE CONTRACTORS

Aerospace Corp
ATTN: V. Josephson
ATTN: T. Salmi
ATTN: I. Garfunkel
ATTN: J. Straus
ATTN: D. Olsen
ATTN: R. Slaughter

Analytical Systems Engineering Corp
ATTN: Radio Sciences

Analytical Systems Engineering Corp
ATTN: Security

BDM Corp
ATTN: L. Jacobs
ATTN: T. Neighbors

Berkeley Research Associates, Inc
ATTN: C. Prettie
ATTN: J. Workman
ATTN: S. Brecht

Boeing Aerospace Co
ATTN: MS/87-63, D. Clauson

Boeing Co
ATTN: G. Hall
ATTN: S. Tashird

BR Communications
ATTN: J. McLaughlin

University of California, San Diego
ATTN: H. Booker

Charles Stark Draper Lab, Inc
ATTN: A. Tetewski
ATTN: D. Cox
ATTN: J. Gilmore

Computer Sciences Corp
ATTN: F. Eisenbarth

COMSAT Labs
ATTN: D. Fang
ATTN: G. Hyde

Cornell University
ATTN: D. Farley Jr
ATTN: M. Kelly

E-Systems, Inc
ATTN: R. Berezdivin

Electrospace Systems, Inc
ATTN: P. Phillips
ATTN: H. Logston

DEPARTMENT OF DEFENSE CONTRACTORS (Continued)

EOS Technologies, Inc
ATTN: B. Gabbard

ESL, Inc
ATTN: J. Lehman
ATTN: R. Hechman
ATTN: R. Ibaraki
ATTN: E. Tsui
ATTN: J. Marshall

General Electric Co
ATTN: C. Zierdt
ATTN: A. Steinmayer

General Electric Co
ATTN: G. Millman

General Research Corp
ATTN: B. Bennett

Geo-Centers, Inc
ATTN: E. Marram

Harris Corp
ATTN: E. Knick

Honeywell, Inc
ATTN: G. Collyer
ATTN: G. Terry

Horizons Technology, Inc
ATTN: R. Kruger

HSS, Inc
ATTN: D. Hansen

IBM Corp
ATTN: H. Ulander

Institute for Defense Analyses
ATTN: E. Bauer
ATTN: H. Wolfhard
ATTN: J. Aein
ATTN: H. Gates

International Tel & Telegraph Corp
ATTN: Technical Library

International Tel & Telegraph Corp
ATTN: G. Wetmore

JAYCOR
ATTN: J. Sperling

Johns Hopkins University
ATTN: J. Newland
ATTN: T. Evans
ATTN: P. Komiske
ATTN: J. Phillips

Kaman Sciences Corp
ATTN: T. Stephens

Kaman Tempo
ATTN: J. Devore
ATTN: B. Gambill
ATTN: DASIAC
ATTN: K. Schwartz
ATTN: W. McNamara
ATTN: W. Knapp

DEPARTMENT OF DEFENSE CONTRACTORS (Continued)

Litton Systems, Inc
ATTN: B. Zimmer

Lockheed Missiles & Space Co, Inc
ATTN: R. Sears
ATTN: J. Kumer

Lockheed Misssiles & Space Co, Inc
ATTN: C. Old
ATTN: D. Churchill
ATTN: Dept 60-12

MIT Lincoln Lab
ATTN: D. Towle

MA/COM Linkabit Inc
ATTN: I. Jacobs
ATTN: A. Viterbi
ATTN: H. Van Trees

Magnavox Govt & Indus Electronics Co
ATTN: G. White

Martin Marietta Corp
ATTN: R. Heffner

McDonnel Douglas Corp
ATTN: R. Halprin
ATTN: H. Spitzer
ATTN: Tech Library Svcs
ATTN: W. Olson

Meteor Communications Corp
ATTN: R. Leader

Mission Research Corp
ATTN: R. Bigoni
ATTN: Tech Library
ATTN: R. Kilb
ATTN: G. McCartor
ATTN: F. Guigliano
ATTN: R. Bogusch
ATTN: S. Gutsche
ATTN: F. Fajen
ATTN: R. Hendrick
ATTN: C. Lauer

Mitre Corp
ATTN: A. Kymmel
ATTN: MS J104/M, R. Dresp
ATTN: G. Harding
ATTN: C. Callahan

Mitre Corp
ATTN: W. Foster
ATTN: M. Horrocks
ATTN: J. Wheeler
ATTN: W. Hall

Pacific-Sierra Research Corp
ATTN: E. Field Jr
ATTN: H. Brode, Chairman SAGE
ATTN: F. Thomas

Pennsylvania State University
ATTN: Ionospheric Research Lab

Photometrics, Inc
ATTN: I. Kofsky

DEPARTMENT OF DEFENSE CONTRACTORS (Continued)

Physical Dynamics, Inc
ATTN: E. Fremouw

Physical Research, Inc
ATTN: R. Deliberis

R&D Associates
ATTN: W. Wright
ATTN: P. Turco
ATTN: R. Lelevier
ATTN: W. Karzas
ATTN: C. Greifinger
ATTN: F. Gilmore
ATTN: H. Ory
ATTN: M. Gantsweg

R&D Associates
ATTN: B. York

Rand Corp
ATTN: C. Crain
ATTN: E. Bedrozian

Riverside Research Institute
ATTN: V. Trapani

Rockwell International Corp
ATTN: R. Buckner

Rockwell International Corp
ATTN: S. Quilici

Santa Fe Corp
ATTN: D. Paolucci

Science Applications, Inc
ATTN: C. Smith
ATTN: E. Straker
ATTN: D. Hamlin
ATTN: L. Linson

Science Applications, Inc
ATTN: J. Cockayne

Stewart Radiance Lab
ATTN: J. Ulwick

DEPARTMENT OF DEFENSE CONTRACTORS (Continued)

Sylvania Systems Group
ATTN: W. Steinhoff

Utah State University
ATTN: I. Hurt
ATTN: R. Baker, Dir Atmos & Space Science
ATTN: L. Jensen, Elec Eng Dept
ATTN: A. Steed

Sylvania Systems Group
ATTN: I. Kohlberg
ATTN: J. Concordia

Technology International Corp
ATTN: W. Boquist

TRI-COM, Inc
ATTN: D. Murray

TRW Electronics & Defense Sector
ATTN: S. Kirchner
ATTN: R. Plebuch

VisiDyne, Inc
ATTN: C. Humphrey
ATTN: W. Reidy
ATTN: J. Carpenter
ATTN: O. Shepard

SRI International
ATTN: G. Price
ATTN: W. Chesnut
ATTN: M. Baron
ATTN: D. McDaniels
ATTN: D. Neilson
ATTN: R. Livingston
ATTN: R. Leadabrand
ATTN: A. Burns
ATTN: J. Petrickes
ATTN: G. Smith
ATTN: W. Jaye
ATTN: V. Gonzales
ATTN: C. Rino
4 cy ATTN: R. Tsunoda
4 cy ATTN: J. Vickrey


DATE
ILME